Biochar as a Renewable Substitute for Carbon Black in Lithium-Ion Battery Electrodes

Seth Kane[a], Aksiin Storer[b], Wei Xu[b], Cecily Ryan[a], and Nicholas P. Stadie[b]*

[a]Department of Mechanical & Industrial Engineering, Montana State University, Bozeman, MT 59717, United States

[b]Department of Chemistry & Biochemistry, Montana State University, Bozeman, MT 59717, United States

*Corresponding Author: nstadie@montana.edu

ABSTRACT Lignin-derived biochar was prepared and characterized towards potential applications as a conductive electrode additive and active lithium host material within lithium-ion batteries (LIBs). This biochar was specifically selected for its high electrical conductivity, which is comparable to that of common conductive carbon black standards (e.g., Super P). Owing to its high electrical conductivity, this biochar serves as an effective conductive additive within electrodes comprised of graphite as the active material, demonstrating slightly improved cell efficiency and rate capability over electrodes using carbon black as the additive. Despite its effectiveness as a conductive additive in LIB anodes, preliminary results show that the biochar developed in this work is not suitable as a direct replacement for carbon black as a conductive additive in $LiFePO_4$ (LFP) cathodes. This latter insufficiency may be due to differences in particle

geometry between biochar and carbon black; further optimization is necessary to permit the application of biochar as a general-purpose conductive additive in LIBs. Nevertheless, these investigations combined with an assessment of greenhouse gas emissions from biochar production show that replacing carbon black with biochar can be an effective method to improve the sustainability of LIBs.

KEYWORDS

Electrical conductivity, graphitic carbon, lignin-derived biocarbon, anode, cathode, electrochemical energy storage, conductive additive.

INTRODUCTION.

The wider application of electrochemical energy storage devices, especially lithium-ion batteries (LIBs), is a critical component of strategies to reduce the global reliance on fossil fuels and slow global warming. However, several fossil-fuel-derived products are still commonly used in fabricating most LIBs, including artificial graphite and carbon black, along with several other minor components. In addition to being derived from fossil fuels, producing these materials results in greenhouse gas emissions of up to 2.4 kg CO_2 equivalent per kg carbon black or up to 4.4 kg CO_2 equivalent per kg artificial graphite.[1,2] In order to make LIBs more sustainable and less reliant on fossil-fuel-derived chemicals, the development of high-performance carbon materials from renewable feedstocks is needed.

A possible alternative to petroleum-derived graphite and carbon black is high-temperature biochar. Biochar is produced by the pyrolysis of biomass, resulting in a solid, carbonaceous powder (similar materials are also referred to as biocarbon, carbonized biomass, activated carbon, non-graphitized carbon, and char).[3,4] The physicochemical properties of biochar, and therefore the inherent electrical conductivity, vary depending on the feedstock and pyrolysis conditions used. With optimal processing conditions, biochar can be produced with comparable chemical composition and electrical properties to commercial carbon black.[5–9] In particular, biochar produced from lignin feedstocks shows higher biochar yields and electrical conductivity than that produced from other biomass precursors.[6,10] Further, lignin is a well-known waste byproduct of the papermaking industry and biorefinery processes; upcycling waste lignin into a valuable product can improve the sustainability of these industries and advance the circular economy.[11]

Biochar has previously been studied as an alternative active material to graphite in the anode of LIBs.[9,12,13] Like other synthetic disordered carbons (e.g., activated carbons), biochar can

be produced that exhibits higher specific capacity than graphite via increased surface and edge adsorption in a "house of cards" type model of capacitive ion storage.[14] The performance of biochar as an active anode material is dependent on the electrical conductivity, graphitic structure, porosity, and chemical composition of the biochar.[10,15] Specifically for lignin-derived biochar, varying performance has been reported depending on the source of the lignin, pyrolysis conditions, and pre- and post-pyrolysis processing.[10,16–19] Despite strong interest in biochar as an active material, little attention has been given to biochar as an alternative conductive additive in the anode or cathode of LIBs, which typically account for up to 10% of the total mass of the electrode. In fact, all previous studies applying biomass-derived carbon as the active material in LIBs still use petroleum-derived carbon black as the conductive additive. The similar disordered graphitic structure and electrical conductivity of biochar to carbon black demonstrate its potential as an alternative to carbon black in electrode applications.[5–8]

Herein, we evaluate the use of high electrical conductivity biochar as both the conductive additive and active electrode material in the graphite anode of standard LIBs and compare biochar against a standard conductive additive (Super P carbon black) and active material (artificial graphite). Biochar was produced by direct pyrolysis at 1100 °C from alkali lignin isolated from hybrid-poplar wood. Preliminary work was also carried out to determine the efficacy of the same biochar as a conductive additive within a standard $LiFePO_4$ (LFP) cathode, as well as the reductions in greenhouse gas emissions associated with replacing carbon black with biochar. Based on the similar electrical conductivity of biochar and Super P, we hypothesized that highly conductive lignin-derived biochar would be an effective and renewable alternative for carbon black as a conductive additive without needing to alter any of the processing conditions or other components of the LIB. The results shed insight into the role of particle size and shape, in addition

to inherent materials properties as playing a crucial role in permitting the use of biochar as a conductive additive in LIBs.

EXPERIMENTAL METHODS.

Materials

A benchmark, high-performance commercial graphite with extensively reported electrochemical properties[20] was obtained from Sigma-Aldrich (product #282863, 20 μm nominal particle size) as a standard active anode material. Two commercial carbon blacks were obtained for comparison to biochar: Super P (Timcal Ltd.) and Vulcan XC-72R (Cabot Corp.). A standard active cathode material, $LiFePO_4$ (LFP) was obtained from MTI Corp. (battery grade, median diameter: 3.5 ± 1.0 μm).

The following materials were used in the preparation of electrochemical cells: lithium hexafluorophosphate ($LiPF_6$, battery grade, Gotion Inc.), ethylene carbonate (EC, battery grade, Gotion Inc.), ethylmethyl carbonate (EMC, battery grade, Gotion Inc.), fluoroethylene carbonate (FEC, battery grade, Gotion Inc.), lithium metal (chips, 99.9%, MTI Corp.), glass microfiber discs (0.67 × 257 mm, GF/D grade, catalog number 1823-257, Whatman), polyvinylidene fluoride (PVDF, 99.5%, MTI Corp.), N-methyl-2-pyrrolidone (NMP, 99.0%, Sigma-Aldrich), copper foil (thickness: 9 μm, MTI Corp.), and aluminum foil (thickness: 15 μm, MTI Corp.).

Biochar Synthesis

Lignin was isolated from an NM-6 hybrid poplar genotype with an alkaline pre-extraction treatment at 95 °C, as previously described.[21] To reduce moisture content, the so-isolated lignin was stored in a drying oven at 105 °C for at least 24 h prior to pyrolysis. Biochar was produced by

the pyrolysis of 1 g of lignin in an alumina boat (100 mm × 20 mm × 13 mm) within a tube furnace fitted with an alumina work tube (Mini Mite, Lindberg/Blue M) under nitrogen atmosphere.[22] The heating zone was purged at 100 mL min^{-1} for 10 min prior to heating; the flow was reduced to 30 mL min^{-1} during pyrolysis. The furnace temperature was ramped at 10 °C min^{-1} to a maximum temperature of 1100 °C, held at the setpoint for 1 h, then allowed to cool to room temperature. After pyrolysis, the resulting biochar was triple washed with deionized water to dissolve sodium sulfate impurities and then dried at 105 °C. To reduce particle size, the biochar was then ball-milled (Mixer Mill 400, Retsch) at 30 Hz (1800 rpm) for 2.5 min with a 50 mL steel jar and a 25 mm steel ball, and then stored in a drying oven at 105 °C until use.

Materials Characterization

Fourier transform infrared spectroscopy (FTIR) was performed using a Thermo Fisher Nicolet iS10 FTIR spectrometer with a Smart iTX ATR accessory employing a diamond crystal. FTIR spectra were collected between 600-4000 cm^{-1} at a resolution of 4 cm^{-1} and with 64 scans per sample and analyzed using SpectraGryph software (v. 1.2.14, Friedrich Menges Software-Entwicklung). Raman spectroscopy was performed using a Horiba LabRam HR Evolution spectrometer outfitted with a confocal microscope. Raman spectra were collected using a 50× long working distance objective, 1800 gr/mm grating, and by irradiation with a frequency-doubled Nd:YAG laser (532 nm) operated at 1-10 mW. The spectra were fitted and analyzed as described elsewhere.[23] X-ray diffraction (XRD) was measured using a Bruker D8 Advance powder X-ray diffractometer with Cu $K\alpha_{1,2}$ radiation. XRD patterns were collected between 5-80° in 2θ using a step size of 0.02° per step. Scanning electron microscopy (SEM) was performed using a Zeiss Supra 55VP field-emission SEM operated at 1 kV with an SE2 detector, with a working distance of approximately 7.5 mm. Energy-dispersive X-ray spectroscopy (EDX) was performed during

SEM using an Oxford Xplore detector. EDX spectra were measured at 250× magnification with a working distance of 8.4 mm. Biochar and carbon black particle size distributions were measured with ~100 mg of material using a Malvern 3000 laser diffraction particle size analyzer with distilled water as a dispersant.

Direct current (DC) electrical conductivity was measured under compression using a guard electrode setup as described in detail elsewhere.[24] Typically, 150 mg of biochar or carbon black was placed in the sample holder, and resistivity measurements were performed every 0.0127 cm (0.005 in) upon compression from the lower current limit of the source meter (Keithly 2450) until further compression could not be applied. All electrical conductivity measurements were performed in triplicate.

Electrode and Cell Fabrication

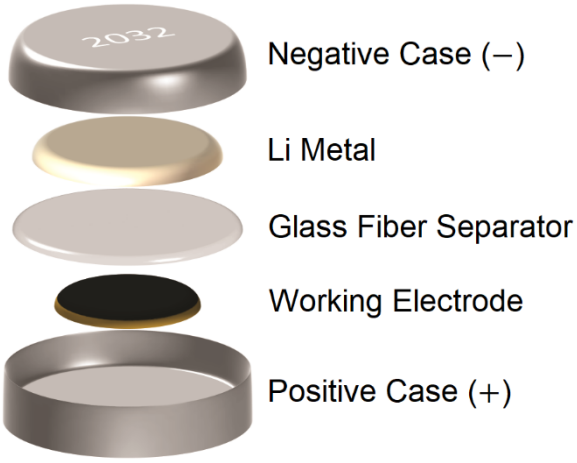

Figure 1. Schematic of electrochemical cell assembly. See Table 1 for different prepared compositions of the carbon electrode.

Seven different permutations of electrode composition were prepared, employing either graphite, LFP, or biochar as the active material and Super P, biochar, or no material as the conductive additive, as shown in Table 1. First, slurries were prepared by hand-grinding the active material (80 wt.%) with conductive additive (10 wt.%) and polyvinylidene fluoride (PVDF) as a

binder (10 wt.%) in NMP as the solvent. In slurries where no conductive additive was used, the weight of the conductive additive was replaced with the active material. Next, the so-obtained slurry was uniformly cast onto a metal foil current collector using the doctor blade technique, dried at 80 °C for 12 h, and then transferred to a vacuum oven at 100 °C for an additional 12 h to remove moisture and solvent. Copper foil was used for electrodes containing graphite or biochar as the active material, while aluminum foil was used for electrodes with LFP as the active material. The resulting electrode was cut into disks with a diameter of 10 mm, with uniform loadings of 2.5-3.0 mg cm^{-2} (±0.2 mg cm^{-2}). Coin cells (316 stainless steel, 2032 format) were assembled in an argon-filled glove box in a two-electrode configuration with lithium metal serving as the counter and reference electrode, a glass microfiber disc as the separator, and a solution of 1.2 M $LiPF_6$ in EC/EMC (3:7, by weight) with 2 wt.% FEC as the electrolyte (125 µL per cell) as shown in Figure 1.

Table 1. Cell compositions (by weight) in this study.

		Active Material		
		Graphite	**Biochar**	**LFP**
Conductive Additive	**Super P**	80% Graphite 10% Super P	80% Biochar 10% Super P	80% LFP 10% Super P
	Biochar	80% Graphite 10% Biochar	90% Biochar	80% LFP 10% Biochar
	(none)	90% Graphite	90% Biochar	N/A

Note: all cells contained 10% PVDF binder as the remaining portion by weight.

Electrochemical Characterization

Galvanostatic charge and discharge (GCD) profiles were measured in half-cell configuration for all cells using a battery cycler (CT30001A, Landt Instruments) within an incubator oven held at a constant temperature of 25.0 °C. For graphite and biochar as the active material, the lithiation process (discharging) was measured using a two-step constant current constant voltage (CCCV) protocol, and the delithiation process (charging) was measured using a single-step constant current (CC) protocol, between 0.05-1.5 V vs. Li/Li^+. A CC formation cycle was first performed at a current rate of 0.1 C (where the C rate is defined as 370 mA g^{-1} for both graphite and biochar) and then allowed to rest for 5 min before further cycling. For LFP as the active material, lithiation (charging) was measured using a CCCV protocol, and delithiation (discharging) was measured using a CC protocol, between 2.0-4.0 V vs. Li/Li^+. In all cases, five initial cycles were carried out at 0.2 C (for a total of 5 h during CCCV discharge) to establish a robust electrode-electrolyte interphase. The rate capability of each electrode was evaluated at current rates of 2 C, 4 C, 6 C, 8 C, 10 C, 20 C, and 40 C. The CCCV lithiation of graphite and biochar was performed until the total discharging time was 30, 15, 10, 7.5, 6, 3, or 2 min, respectively. Electrochemical impedance spectroscopy (EIS) was measured both in situ (in newly formed cells) and ex situ (on bare electrodes never cycled within a coin cell). For ex situ measurements, spectra were collected using a four-point probe to reduce the impact of system resistance, system inductance, and contact resistance using a Gamry Reference 600 potentiostat from 0.1 Hz to 100 kHz with an applied voltage of 0.5 mV.

RESULTS & DISCUSSION.

Biochar Characterization

The biochar produced in this study (referred to in previous work as HL1100[6]) shows comparable electrical conductivity (9.1±0.89 S cm^{-1}) to the commercial carbon black powders commonly employed as the conductive additive in LIBs: Super P (7.959±3.1 S cm^{-1}) and Vulcan XC-72R (6.9±2.0 S cm^{-1}) (Figure 2a). The carbon structure contributing to this electrical conductivity was explored using Raman spectroscopy and XRD. All three materials show broad D (~1340 cm^{-1}) and G (~1580 cm^{-1}) peaks in their Raman spectra, indicating nanocrystalline graphitic structure with significant disorder. Importantly, all three materials exhibit a similar G peak width of ~116 cm^{-1} at the half-maximum and a D:G intensity ratio of ~1.0 (Figure 2b). Similarly, XRD patterns of all three materials show the presence of broad (002) and (10*l*) reflections characteristic of turbostratic graphite (Figure 2c). In biochar and both carbon black materials, the (002) reflection is shifted to a lower angle than pristine graphite, indicating increased interlayer distance. As a subtle difference, the biochar exhibits a more prominent (10*l*) family of reflections than either of the carbon black materials and a slightly lower D:G ratio, indicating higher in-plane ordering. Hence, biochar's slightly higher electrical conductivity can be attributed to the existence of larger graphene domains than carbon black despite similar or perhaps poorer ordering along the stacking direction.

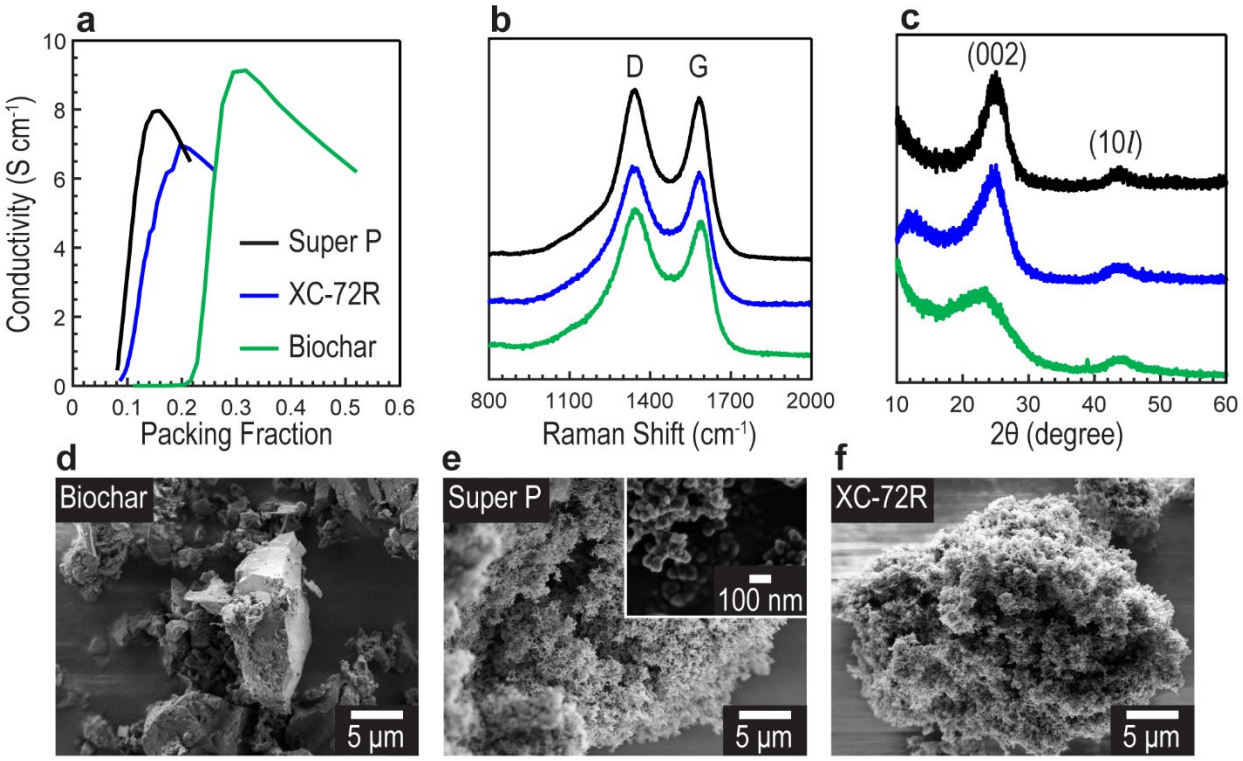

Figure 2. Materials properties of biochar compared to two commercial carbon black materials: Super P and Vulcan XC-72R. (a) Mean electrical conductivity as a function of packing fraction (the shaded region represents one standard deviation based on triplicate analysis). (b) Raman spectra as measured at an incident wavelength of 532 nm. (c) XRD patterns. (d-f) SEM micrographs at 6000× magnification (inset at 225k× magnification).

Despite similarities in electrical conductivity and graphitic structure, important differences in the particle morphology between biochar and the two carbon materials were observed upon electron microscopy investigation. A distinctively textured ("fluffy") surface structure was observed for Super P and Vulcan XC-72R (Figure 2e-2f). This structure is a result of the nodule-aggregate-agglomerate structure of carbon black wherein small (<100 nm) carbon black nodules (primary particles, inset in Figure 2e) form larger (<1 μm) aggregates that cluster into 10-20 μm agglomerates.[25] In contrast, biochar exhibits a more prismatic structure with smooth surfaces due to the ball-milling that was performed to reduce particle size (Figure 2d). While biochar appears

to have a smaller median particle size of 8.7 μm than either carbon black (17.6 and 14.5 μm for Super P and Vulcan XC-72R, respectively, Figure S2), these particle sizes do not account for deagglomeration during mixing.[25,26] As a result of these morphological differences, biochar has a higher unpacked bulk density than either carbon black, resulting in a higher electrical percolation threshold (Figure 2a). When considering chemical composition, EDX measurements indicate that biochar has higher oxygen content than either carbon black (Figure S2). This oxygen content is directly proportional to defects within the graphitic carbon structure.[4] Before washing to remove inorganic impurities, sodium and sulfur were also observed in the biochar; FTIR and XRD reveal this as sodium sulfate (Na_2SO_4) (Figure S2). Past studies have differed in their interpretation of the role that sodium sulfate plays during pyrolysis to produce biochar. Some studies hypothesize that sodium sulfate catalyzes the formation of graphitic structures, while other studies propose that sodium sulfate inhibits it.[27–29] After washing, limited sodium, and sulfur remain in the biochar, and no XRD peak corresponding to Na_2SO_4 is present (Figure S2).

The biochar prepared in this work shows similar properties to highly conductive biochars produced in past studies. A review of 52 biochars produced at pyrolysis temperatures between 900-1400 °C from various feedstocks showed an average electrical conductivity of 12.7 S cm^{-1}, with a wide range of electrical conductivities from 0.1-95 S cm^{-1}.[6] The biochar characterized herein is similar in electrical conductivity to the aforementioned average. Only a limited increase in electrical conductivity is observed after pyrolysis above 1100 °C, as full percolation between graphitic crystallites can be achieved.[30] Biochars prepared in previous work also exhibit similar structure, with Raman D:G ratios of ~1 when characterized using 532 nm incident radiation and broad (002) and (10*l*) XRD reflections.[31–33] The graphite used in this study has been extensively characterized in past work, referred to therein as AG20.[20]

Electrochemical Characterization

Electrochemical characterization of biochar compared to graphite within a half-cell configuration and using a standard LIB electrolyte is shown in Figure 3. At low current rates, the GCD profiles (Figure 3a) show that the typical staging features associated with the lithiation and delithiation of pristine graphite are lacking for the more disordered biochar. Most of the capacity in biochar is found within the sloped region of the GCD profile, which is consistent with a capacitive mechanism of charge storage typical of hard carbons.[14] At high current rates (using a CCCV lithiation protocol), the biochar displays nearly identical CCCV capacity to graphite (Figures 2b-2d). For example, both biochar and graphite display capacities of ~160 and ~120 mAh g^{-1} at 4 C and 10 C rates, respectively. The similar capacity for both materials indicates that at high rates, charge storage at the electrode interface becomes dominant owing to limitations in ion mobility originating from higher charge transfer resistance and solid-state diffusion within the graphite galleries. However, at low rates (0.2 and 2 C), graphite exhibits a much higher capacity than biochar as an active material (Figure 3a). This low-rate performance indicates that the biochar has a relatively low surface area accessible for ion adsorption compared to the inner "surface area" of the graphite galleries. There is no meaningful difference in Coulombic efficiency between graphite and biochar within this electrochemical protocol (Figure 3e).

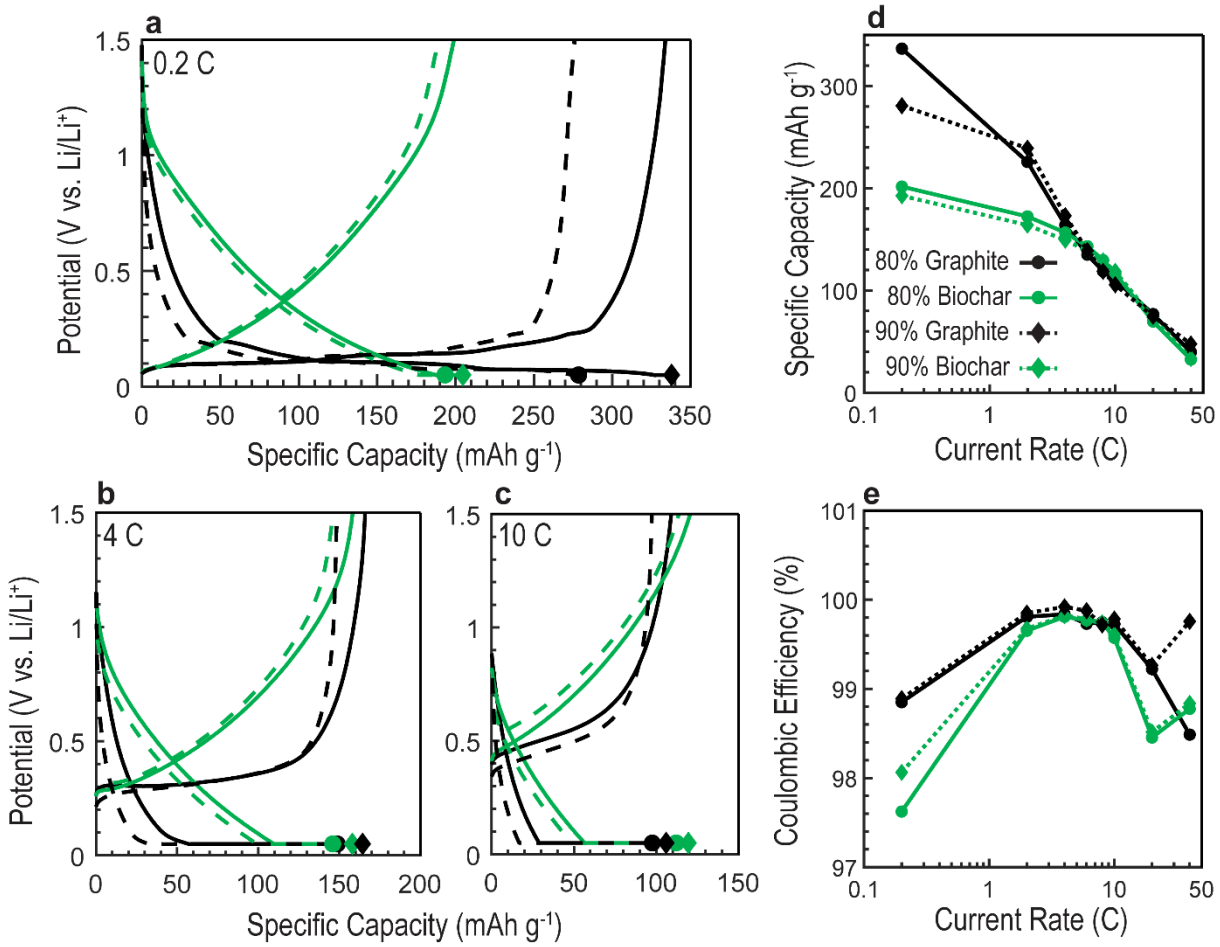

Figure 3. Comparison of biochar and artificial graphite as the active material in the anode of LIBs, with (80% active material) and without (90% active material) Super P conductive additive. Representative GCD profiles for graphite and biochar at charging rates of (a) 0.2 C, (b) 4 C, and (c) 10 C, with points indicating maximum discharge specific capacity prior to CCCV cutoff (additional measurements are shown in Figures S3 and S4 and in Table S1). Rate capability measurements of graphite and biochar showing (d) capacity and (e) Coulombic efficiency for charging rates from 0.2 C to 40 C.

Conductive Additive in LIB Anodes

Comparisons of biochar and super P as a conductive additive via GCD cycling and rate capability investigations show only minor differences between the two materials (Figure 4). There is no significant difference in the capacity of graphite measured at 0.2 C in the presence of either conductive additive (Figure 4a); the average specific capacity was 329.2±1.4 mAh g^{-1} for electrodes containing biochar and 336.5±1.0 mAh g^{-1} for electrodes containing Super P. This reduction in capacity can be observed in the discharge curve, where cells with biochar as the conductive additive reach the CC voltage cutoff (0.05 V) at a slightly lower capacity than Super P cells (Figure 4a, inset). The rate capability measurements at up to 40 C corroborate previous results[34] that the specific type of graphite chosen for this work exhibits excellent performance at extremely high current rates when combined with a conductive additive. In the extremely high current rate regime, the capacity of graphite declines to ~77 mAh g^{-1} at 20 C and ~40 mAh g^{-1} at 40 C in the presence of both additives, though slightly higher with biochar than Super P. In the final measurements at 2 C, electrodes with biochar as the conductive additive exhibit a marginal increase in capacity (237±16 mAh g^{-1}) relative to electrodes containing Super P (209±20 mAh g^{-1}). All cells with either biochar or Super P as the conductive additive display a Coulombic efficiency of ~100% at current rates from 2-10 C (Figure 4c). Together, these results indicate that the biochar developed herein yields comparable performance as a standard conductive additive, Super P, commonly used in commercial LIBs. This is further supported by four-point impedance measurements of the ex situ electrodes, where electrodes with biochar as the conductive additive exhibit lower impedance (0.0006 Ω) than identical electrodes prepared with carbon black (0.004 Ω) in the frequency range of 10^{-1} to 10^{2} Hz (Figure S6).

The above results show that a 10 wt.% addition of biochar or Super P permits the full cycling of graphite at low current rates (0.2 C), where without any conductive additive, the performance of graphite is reduced by 17%. However, at higher rates, a similar capacity is found in cells with or without conductive additive. This difference can be attributed to a change in the primary charge storage mechanism at low and high current rates. At 0.2 C, the charge storage mechanism is primarily faradaic, and the electrical conductivity contributed by the conductive additive is needed to ensure connectivity of the entire electrode mass. At faster rates, the charge storage mechanism shifts to primarily capacitive. The similar behavior at higher current rates indicates that the electrode mass available for ion adsorption as opposed to intercalation is the same regardless of the presence of additive. Accordingly, cells with biochar as the active material exhibit a less significant decrease in low-current capacity in the absence of conductive additive than cells with graphite.

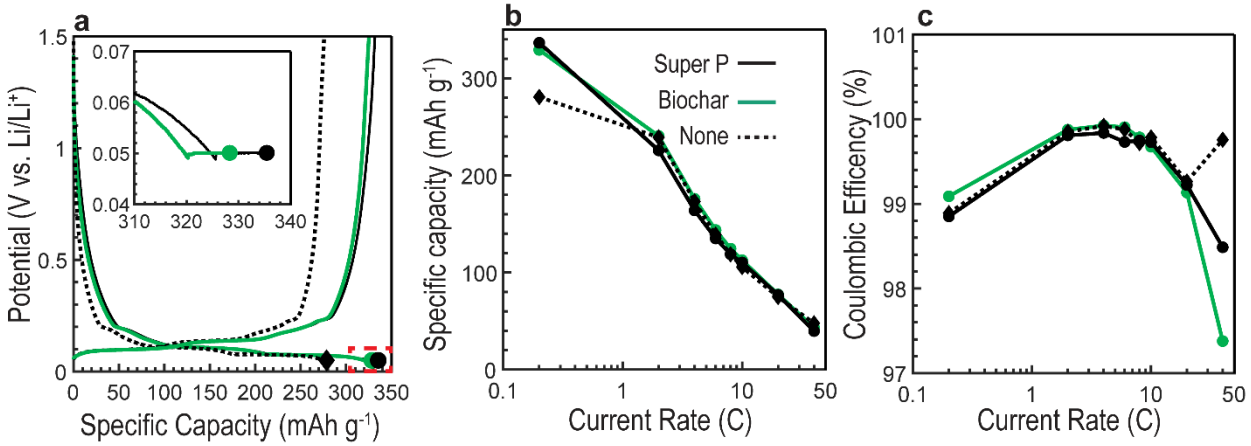

Figure 4. Comparison of Super P and biochar as the conductive additive in the anode of LIBs, with 80% graphite, 10% Super P or biochar, and 10% PVDF. (a) GCD profiles of graphite at 0.2 C. The inset highlights the region of maximum lithiation prior to CCCV cutoff (shown by the red box), with marked points indicating maximum discharge specific capacity prior to CCCV cutoff (additional measurements are shown in Figure S5 and in Table S2). Rate capability measurements of graphite showing (b) capacity and (c) Coulombic efficiency for charging rates from 0.2 C to 40 C.

Conductive Additive in LIB Cathodes

In contrast to its effective application as a conductive additive in graphite-based LIB anodes, biochar was not found to be an effective additive within LFP-based cathodes in this work (Figure S7). Half-cells containing a standard commercial LFP powder as the active material and biochar as the conductive additive in the working electrode exhibited no capacity. In contrast, control cells with Super P as the conductive additive exhibited a reversible capacity of 170 mAh g^{-1} at 34 mA g^{-1} (both normalized per mass of LFP). We hypothesize that this result is due to two major differences between biochar and Super P: the higher density of biochar and the fluffy morphology of Super P (a property it shares with other carbon blacks, such as Vulcan XC-72R). In electrodes, the effective size of carbon black is observed to be smaller than biochar for both graphite and LFP-based electrodes (Figure S9). In graphite-based electrodes, this difference in particle size may not play an important role, due to both the higher electrical conductivity of graphite, and larger particle size of graphite relative to both carbon black and biochar. However, in LFP-based electrodes, biochar is observed to be much larger than LFP particles, resulting in ineffective dispersion and bridging between particles. In contrast, carbon black is observed to be both smaller than LFP particles and well dispersed between LFP particles.

Together, these differences result in a higher electrical percolation threshold for biochar than Super P. This higher percolation threshold was observed in the packed powder electrical conductivity measurements presented herein (Figure 2a) and has also been previously observed for electrically conductive biochar in polymer composites.[35] This finding is further supported by ex situ four-point EIS measurements of the cathodes, which reveal that the impedance of the biochar-containing electrodes (>1.5 GΩ) is many orders of magnitude larger than that of Super P-containing electrodes (0.07 Ω, Figure S8). This limitation to the application of biochar as a

universal conductive additive may highlight the importance of the fluffy particle structure of Super P. The texture of both Super P and Vulcan XC-72R is composed of small (<100 nm) nodules formed during spray pyrolysis, giving both materials a high void volume and low unpacked density.[36] When dispersed in the PVDF binder, this fluffy structure results in a reduced percolation threshold relative to the compact structure of biochar. Further investigation is necessary to understand how the biochar production process can be modified to combat this issue, whether by modifying the synthesis conditions or post-synthetic processing.

Greenhouse Gas Emissions Assessment

The production of an effective conductive additive for battery electrodes from lignin presents as a more sustainable alternative to the spray pyrolysis of fossil-fuel-derived chemicals. However, to date, no comprehensive study has been performed to determine the environmental impacts of biochar produced at temperatures higher than 900 °C. While a comprehensive life cycle assessment is outside the scope of this study, the global warming potential of production of 1 kg of biochar is estimated with the system boundary shown in Figure S1. This estimate is based on the original carbon content of the lignin (54%), the biochar yield (27.2% or 3.7 kg lignin per kg biochar), and the carbon content of the resulting biochar (83.7%)[6] with the assumption that pyrolysis is net energy neutral[37–39] (more details are provided in the Supporting Information). This value should be compared to the greenhouse gas emissions required to produce 1 kg carbon black (2.4 kg CO_2 equivalent)[2] and that resulting from the atmospheric combustion of 3.7 kg lignin (7.7 kg CO_2 equivalent) which results in the additional production of 36.2 MJ of electricity.[40] The production of 1 kg of biochar results in net greenhouse gas emissions of 1.2 kg CO_2 equivalent, with additional emissions of 3.9 kg CO_2 equivalent produced to replace the energy that otherwise would be produced by combustion of the 3.7 kg lignin.[41] This results in a total estimated emission

of 5.1 kg for the production of 1 kg of biochar, compared to 10.0 kg for the production of 1 kg of carbon black and the combustion of 3.7 kg of lignin. The net change in emissions from producing biochar from lignin rather than combusting lignin is -0.657 kg CO_2 equivalent per kg of lignin. Therefore, the use of biochar rather than carbon black is estimated to reduce emissions by 4.9 kg CO_2 equivalent per kg of conductive additive used, a reduction of 49%. This decrease is primarily due to two factors: the production of biochar resulting in lower emissions (1.2 kg CO_2 equivalent) than the production of carbon black (2.4 kg CO_2 equivalent) and that energy produced by the combustion of lignin results in more emissions (0.209 kg CO_2 eq. MJ^{-1}) than the electricity grid (taken herein as the average emissions associated with the electrical grid in the United States in 2020: 0.108 kg CO_2 eq. MJ^{-1}).[41]

While no studies to date have examined the environmental impacts of high-temperature biochar, past studies have found the global warming potential of biochar production to increase linearly as temperature increases between 300-600 °C.[42] When this relationship is extrapolated to biochar produced at 1100 °C, a net global warming potential of -0.134 kg CO_2 equivalent per kg feedstock is estimated. This result is comparable to the estimate of -0.657 kg CO_2 equivalent per kg lignin derived herein, when not including the avoided impacts of carbon black production. A complete life cycle assessment, including other environmental impact factors and the application and end-of-life stages of the material, is needed to fully compare the environmental impacts of biochar and carbon black as a conductive additive. Until this is performed, in the production phase, the use of biochar is estimated to reduce the global warming potential of the conductive additive for LIB electrodes relative to carbon black.

Importantly, this estimate assumes that the pyrolysis process is net energy neutral - that the energy requirements of pyrolysis are met by heat, bio-oil, and syngas co-products. This assumption

is well established for lower temperature pyrolysis processes,[37–39] but additional study of high temperature pyrolysis processes is needed to verify this assumption for the materials discussed herein. The reductions in greenhouse gas emissions estimated herein support the environmental benefits of replacing artificial graphite with highly graphitic biochar that have been produced at similar temperatures to those examined in this study.[10] As the materials examined in past studies use similar pyrolysis temperatures and result in similar biochar yields to this study, similar reductions in greenhouse gas emissions are expected to those estimated herein.

Discussion

As hypothesized, the pyrolysis of lignin at 1100 °C results in an electrically conductive biochar that is comparable to a standard carbon black (Super P) as the conductive additive in the graphite anode of LIBs. Slightly poorer capacity was exhibited by biochar-containing cells at low current rates, while slightly higher capacity was exhibited at high current rates, compared to Super P. These results indicate that biochar can be produced by a simple method as an acceptable replacement for carbon black in LIB anodes. However, the failure of the same biochar as a conductive additive in a standard LFP-based LIB cathode demonstrates the limitations of this material in replacing carbon black in all battery electrode compositions. Previous studies have successfully produced biochars with <1 μm particle size via ball milling [5] or "fluffy" morphology via spray pyrolysis[43]. Further investigations of similar approaches may result in a biochar material with a shape and density more similar to carbon black, while maintaining the strong electrical conductivity found in this study, to address the poor percolation behavior of the biochar produced by direct one-pot pyrolysis as investigated herein.

The biochar produced in this study exhibits a lower specific capacity as the active material than that reported for similar materials produced in past studies.[10,17,18] Such differences are likely

owed to a difference in specific surface area (for capacitive-type charge storage) or in crystallinity (for intercalation-type charge storage), both of which can be widely varied by tuning the synthesis conditions. The biochar produced herein was optimized with a focus on maximizing electrical conductivity rather than producing biochar with high surface area or a highly graphitic structure. Hence, the biochar in this study performs well as a conductive additive but foregoes a focus on the role of the additive in increasing the overall capacity of the electrode.

CONCLUSIONS.

Biochar can be produced from lignin with limited processing and demonstrated to be comparable in terms of electrical conductivity and graphitic structure to standard commercial carbon blacks. The particle density and morphology achieved in this work serve biochar well as an effective replacement for carbon black as the conductive additive in the graphite-based anode of LIBs. However, the similar application of biochar in an LFP-based LIB cathode is ineffective, likely owing to its high percolation threshold relative to carbon black. This biochar was selected based on its high electrical conductivity rather than surface area or ordered graphitic structure that has been prioritized in past investigations of biochar as an active electrode material; as a result, this biochar exhibits lower capacity as an active material than materials specifically optimized as an active material in past studies. When combined with past research on bio-based active materials (e.g., highly graphitized biochar),[10,15] this study reveals a path forward to LIBs with only bio-based carbon materials. Such a replacement is estimated to reduce the greenhouse gas emissions associated with the production of conductive additives for battery electrodes by 49% and reduce the reliance on fossil fuel-derived products, improving the sustainability of LIBs without any degradation of battery performance.

ASSOCIATED CONTENT.

Supporting Information. Supporting information to this article is available online and includes additional materials and electrochemical characterization, and details of greenhouse gas emission estimates.

AUTHOR INFORMATION.

Corresponding Author

*nstadie@montana.edu

Author Contributions

The manuscript was written through contributions of all authors. All authors have given approval to the final version of the manuscript.

Funding Sources

Funding for this work was provided by the DEVCOM Army Research Laboratory (ARL) under cooperative agreement (W911NF-20-2-0284). S.K. acknowledges funding through an Environmental Research and Education Foundation Ph.D. Scholarship. A.S. acknowledges funding from the National Science Foundation Research Experiences for Undergraduates (REU) Program (CHE-1852214). This work was performed in part at the Montana Nanotechnology Facility (MONT, an NNCI facility supported by National Science Foundation grant ECCS-1542210).

ACKNOWLEDGMENTS.

We are grateful to the Hodge Laboratory for providing the biochar feedstock.

REFERENCES

(1) Argonne National Laboratory. GREET .Net. 2021.

(2) Fan, Y.; Fowler, G. D.; Zhao, M. The Past, Present and Future of Carbon Black as a Rubber Reinforcing Filler – A Review. *Journal of Cleaner Production* **2020**, *247*, 119115. https://doi.org/10.1016/J.JCLEPRO.2019.119115.

(3) Liu, W. J.; Jiang, H.; Yu, H. Q. Development of Biochar-Based Functional Materials: Toward a Sustainable Platform Carbon Material. *Chemical Reviews* **2015**, *115* (22), 12251–12285. https://doi.org/10.1021/ACS.CHEMREV.5B00195.

(4) McDonald-Wharry, J. S.; Manley-Harris, M.; Pickering, K. L. Reviewing, Combining, and Updating the Models for the Nanostructure of Non-Graphitizing Carbons Produced from Oxygen-Containing Precursors. *Energy and Fuels*. American Chemical Society October 20, 2016, pp 7811–7826. https://doi.org/10.1021/acs.energyfuels.6b00917.

(5) Snowdon, M. R.; Mohanty, A. K.; Misra, M. A Study of Carbonized Lignin as an Alternative to Carbon Black. **2014**. https://doi.org/10.1021/sc500086v.

(6) Kane, S.; Ulrich, R.; Harrington, A.; Stadie, N. P.; Ryan, C. Physical and Chemical Mechanisms That Influence the Electrical Conductivity of Lignin-Derived Biochar. *Carbon Trends* **2021**, *5*, 100088. https://doi.org/10.1016/J.CARTRE.2021.100088.

(7) Vivekanandhan, S.; Misra, M.; Mohanty, A. K. Microscopic, Structural, and Electrical Characterization of the Carbonaceous Materials Synthesized from Various Lignin Feedstocks. *Journal of Applied Polymer Science* **2015**, *132* (15), 41786. https://doi.org/10.1002/APP.41786.

(8) Chatterjee, S.; Clingenpeel, A.; McKenna, A.; Rios, O.; Johs, A. Synthesis and Characterization of Lignin-Based Carbon Materials with Tunable Microstructure. *RSC Advances* **2013**, *4* (9), 4743–4753. https://doi.org/10.1039/C3RA46928J.

(9) Rahman, M. Z.; Edvinsson, T.; Kwong, P. Biochar for Electrochemical Applications. *Current Opinion in Green and Sustainable Chemistry* **2020**, *23*, 25–30. https://doi.org/10.1016/J.COGSC.2020.04.007.

(10) Sagues, W. J.; Yang, J.; Monroe, N.; Han, S. D.; Vinzant, T.; Yung, M.; Jameel, H.; Nimlos, M.; Park, S. A Simple Method for Producing Bio-Based Anode Materials for Lithium-Ion Batteries. *Green Chemistry* **2020**, *22* (20), 7093–7108. https://doi.org/10.1039/D0GC02286A.

(11) Schutyser, W.; Renders, T.; van den Bosch, S.; Koelewijn, S. F.; Beckham, G. T.; Sels, B. F. Chemicals from Lignin: An Interplay of Lignocellulose Fractionation, Depolymerisation, and Upgrading. *Chemical Society Reviews* **2018**, *47* (3), 852–908. https://doi.org/10.1039/C7CS00566K.

(12) Kalinke, C.; de Oliveira, P. R.; Bonacin, J. A.; Janegitz, B. C.; Mangrich, A. S.; Marcolino-Junior, L. H.; Bergamini, M. F. State-of-the-Art and Perspectives in the Use of Biochar for

Electrochemical and Electroanalytical Applications. *Green Chemistry* **2021**, *23* (15), 5272–5301. https://doi.org/10.1039/D1GC00843A.

(13) Liu, W. J.; Jiang, H.; Yu, H. Q. Emerging Applications of Biochar-Based Materials for Energy Storage and Conversion. *Energy & Environmental Science* **2019**, *12* (6), 1751–1779. https://doi.org/10.1039/C9EE00206E.

(14) Dahn, J. R.; Zheng, T.; Liu, Y.; Xue, J. S. Mechanisms for Lithium Insertion in Carbonaceous Materials. *Science (1979)* **1995**, *270* (5236), 590–593. https://doi.org/10.1126/SCIENCE.270.5236.590.

(15) Senthil, C.; Lee, C. W. Biomass-Derived Biochar Materials as Sustainable Energy Sources for Electrochemical Energy Storage Devices. *Renewable and Sustainable Energy Reviews* **2021**, *137*, 110464. https://doi.org/10.1016/J.RSER.2020.110464.

(16) Wu, X.; Jiang, J.; Wang, C.; Liu, J.; Pu, Y.; Ragauskas, A.; Li, S.; Yang, B. Lignin-Derived Electrochemical Energy Materials and Systems. *Biofuels, Bioproducts and Biorefining* **2020**, *14* (3), 650–672. https://doi.org/10.1002/BBB.2083.

(17) Zhang, W.; Yin, J.; Lin, Z.; Lin, H.; Lu, H.; Wang, Y.; Huang, W. Facile Preparation of 3D Hierarchical Porous Carbon from Lignin for the Anode Material in Lithium Ion Battery with High Rate Performance. *Electrochimica Acta* **2015**, *176*, 1136–1142. https://doi.org/10.1016/J.ELECTACTA.2015.08.001.

(18) Tenhaeff, W. E.; Rios, O.; More, K.; McGuire, M. A. Highly Robust Lithium Ion Battery Anodes from Lignin: An Abundant, Renewable, and Low-Cost Material. *Advanced Functional Materials* **2014**, *24* (1), 86–94. https://doi.org/10.1002/ADFM.201301420.

(19) Xi, Y.; Huang, S.; Yang, D.; Qiu, X.; Su, H.; Yi, C.; Li, Q. Hierarchical Porous Carbon Derived from the Gas-Exfoliation Activation of Lignin for High-Energy Lithium-Ion Batteries. *Green Chemistry* **2020**, *22* (13), 4321–4330. https://doi.org/10.1039/D0GC00945H.

(20) Xu, W.; Welty, C.; Peterson, M. R.; Read, J. A.; Stadie, N. P. Exploring the Limits of the Rapid-Charging Performance of Graphite as the Anode in Lithium-Ion Batteries. *Journal of The Electrochemical Society* **2022**, *169* (1), 010531. https://doi.org/10.1149/1945-7111/AC4B87.

(21) Singh, S. K.; Savoy, A. W.; Yuan, Z.; Luo, H.; Stahl, S. S.; Hegg, E. L.; Hodge, D. B. Integrated Two-Stage Alkaline-Oxidative Pretreatment of Hybrid Poplar. Part 1: Impact of Alkaline Pre-Extraction Conditions on Process Performance and Lignin Properties. *Industrial and Engineering Chemistry Research* **2019**, *58* (35), 15989–15999. https://doi.org/10.1021/ACS.IECR.9B01124/SUPPL_FILE/IE9B01124_SI_001.PDF.

(22) Quosai, P.; Anstey, A.; Mohanty, A. K.; Misra, M. Characterization of Biocarbon Generated by High- and Low-Temperature Pyrolysis of Soy Hulls and Coffee Chaff: For Polymer Composite Applications. *Royal Society Open Science* **2018**, *5* (8). https://doi.org/10.1098/RSOS.171970.

(23) McGlamery, D.; Baker, A. A.; Liu, Y. S.; Mosquera, M. A.; Stadie, N. P. Phonon Dispersion Relation of Bulk Boron-Doped Graphitic Carbon. *Journal of Physical Chemistry C* **2020**, *124* (42), 23027–23037. https://doi.org/10.1021/ACS.JPCC.0C06918/SUPPL_FILE/JP0C06918_SI_001.PDF.

(24) Kane, S.; Warnat, S.; Ryan, C. Improvements in Methods for Measuring the Volume Conductivity of Electrically Conductive Carbon Powders. *Advanced Powder Technology* **2021**, *32* (3), 702–709. https://doi.org/10.1016/J.APT.2021.01.016.

(25) Mayer, J. K.; Almar, L.; Asylbekov, E.; Haselrieder, W.; Kwade, A.; Weber, A.; Nirschl, H. Influence of the Carbon Black Dispersing Process on the Microstructure and Performance of Li-Ion Battery Cathodes. *Energy Technology* **2020**, *8* (2), 1900161. https://doi.org/10.1002/ENTE.201900161.

(26) Grießl, D.; Huber, K.; Scherbauer, R.; Kwade, A. Dispersion Kinetics of Carbon Black for the Application in Lithium-Ion Batteries. *Advanced Powder Technology* **2021**, *32* (7), 2280–2288. https://doi.org/10.1016/J.APT.2021.05.003.

(27) Xiao, G.; Ni, M.; Xiao, R.; Gao, X.; Cen, K. Catalytic Carbonization of Lignin for Production of Electrically Conductive Charcoal. *Journal of Biobased Materials and Bioenergy* **2012**, *6* (1), 69–74. https://doi.org/10.1166/JBMB.2012.1190.

(28) Rodríguez-Mirasol, J.; Cordero, T.; Rodríguez, J. J. High-Temperature Carbons from Kraft Lignin. *Carbon N Y* **1996**, *34* (1), 43–52. https://doi.org/10.1016/0008-6223(95)00133-6.

(29) Vivekanandhan, S.; Misra, M.; Mohanty, A. K. Microscopic, Structural, and Electrical Characterization of the Carbonaceous Materials Synthesized from Various Lignin Feedstocks. *Journal of Applied Polymer Science* **2015**, *132* (15). https://doi.org/10.1002/APP.41786.

(30) Rhim, Y. R.; Zhang, D.; Fairbrother, D. H.; Wepasnick, K. A.; Livi, K. J.; Bodnar, R. J.; Nagle, D. C. Changes in Electrical and Microstructural Properties of Microcrystalline Cellulose as Function of Carbonization Temperature. *Carbon N Y* **2010**, *48* (4), 1012–1024. https://doi.org/10.1016/j.carbon.2009.11.020.

(31) Shao, Y.; Guizani, C.; Grosseau, P.; Chaussy, D.; Beneventi, D. Biocarbons from Microfibrillated Cellulose/Lignosulfonate Precursors: A Study of Electrical Conductivity Development during Slow Pyrolysis. *Carbon N Y* **2018**, *129*, 357–366. https://doi.org/10.1016/j.carbon.2017.12.037.

(32) McDonald-Wharry, J. S.; Manley-Harris, M.; Pickering, K. L. Reviewing, Combining, and Updating the Models for the Nanostructure of Non-Graphitizing Carbons Produced from Oxygen-Containing Precursors. *Energy and Fuels*. American Chemical Society October 20, 2016, pp 7811–7826. https://doi.org/10.1021/acs.energyfuels.6b00917.

(33) Saravanan, K. R.; Kalaiselvi, N. Nitrogen Containing Bio-Carbon as a Potential Anode for Lithium Batteries. *Carbon N Y* **2015**, *81* (1), 43–53. https://doi.org/10.1016/J.CARBON.2014.09.021.

(34) Xu, W.; Welty, C.; Peterson, M. R.; Read, J.; Stadie, N. P. Exploring the Limits of the Rapid-Charging Performance of Graphite as the Anode in Lithium-Ion Batteries. *Journal of The Electrochemical Society* **2022**. https://doi.org/10.1149/1945-7111/AC4B87.

(35) Kane, S.; Ryan, C. Biochar from Food Waste as a Sustainable Replacement for Carbon Black in Upcycled and Compostable Composites. *Composites Part C: Open Access* **2022**, *8*, 100274. https://doi.org/10.1016/j.jcomc.2022.100274.

(36) Dannenberg, E. M.; Paquin, L.; Gwinnell, H. Carbon Black. *Kirk-Othmer Encyclopedia of Chemical Technology* **2000**. https://doi.org/10.1002/0471238961.0301180204011414.A01.

(37) KODERA, Y.; KAIHO, M. Model Calculation of Heat Balance of Wood Pyrolysis. *Journal of the Japan Institute of Energy* **2016**, *95* (10), 881–889. https://doi.org/10.3775/JIE.95.881.

(38) Xu, R.; Ferrante, L.; Hall, K.; Briens, C.; Berruti, F. Thermal Self-Sustainability of Biochar Production by Pyrolysis. *Journal of Analytical and Applied Pyrolysis* **2011**, *91* (1), 55–66. https://doi.org/10.1016/J.JAAP.2011.01.001.

(39) Peters, J. F.; Iribarren, D.; Dufour, J. Biomass Pyrolysis for Biochar or Energy Applications? A Life Cycle Assessment. *Environmental Science and Technology* **2015**, *49* (8), 5195–5202. https://doi.org/10.1021/ES5060786/SUPPL_FILE/ES5060786_SI_001.PDF.

(40) Bernier, E.; Lavigne, C.; Robidoux, P. Y. Life Cycle Assessment of Kraft Lignin for Polymer Applications. *International Journal of Life Cycle Assessment* **2013**, *18* (2), 520–528. https://doi.org/10.1007/S11367-012-0503-Y/FIGURES/3.

(41) U.S. Energy Information Administration. *Electricity Data*. https://www.eia.gov/electricity/data.php (accessed 2021-12-29).

(42) Lu, H. R.; el Hanandeh, A. Life Cycle Perspective of Bio-Oil and Biochar Production from Hardwood Biomass; What Is the Optimum Mix and What to Do with It? *Journal of Cleaner Production* **2019**, *212*, 173–189. https://doi.org/10.1016/J.JCLEPRO.2018.12.025.

(43) Kim, J. K.; Yoo, Y.; Kang, Y. C. Scalable Green Synthesis of Hierarchically Porous Carbon Microspheres by Spray Pyrolysis for High-Performance Supercapacitors. *Chemical Engineering Journal* **2020**, *382*, 122805. https://doi.org/10.1016/J.CEJ.2019.122805.

For Table of Contents Use Only

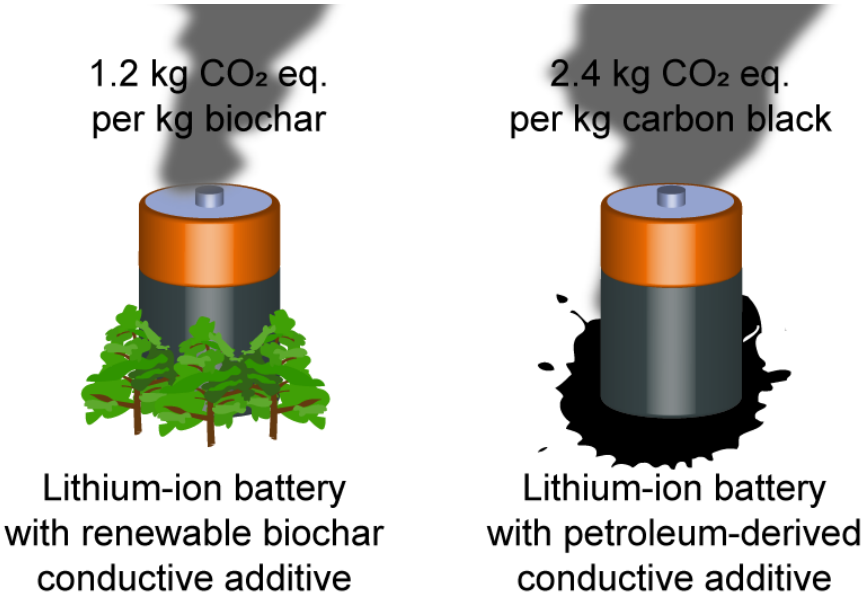

SYNOPSIS

High electrical conductivity biochar can replace standard conductive additives in the anode of lithium-ion batteries with a 49% reduction in greenhouse gas emissions; use in the cathode, however, remains unsuccessful.